Redox Biology 87 (2025) 103871

Contents lists available at ScienceDirect

Redox Biology

journal homepage: www.elsevier.com/locate/redox

Noninvasive *in vivo* discrimination between mitochondrial ROS and global ROS production in solid tumors using EPR spectroscopy

Barbara Mathieu [a,b], Justin D. Rondeau [b], Lionel Mignion [c], Pierre Sonveaux [b,d], Bernard Gallez [a,*]

[a] Biomedical Magnetic Resonance, Louvain Drug Research Institute (LDRI), Université Catholique de Louvain (UCLouvain), 1200, Brussels, Belgium
[b] Pole of Pharmacology and Therapeutics, Institut de Recherches Expérimentales et Cliniques (IREC), Université Catholique de Louvain (UCLouvain), 1200, Brussels, Belgium
[c] Nuclear and Electron Spin Technologies, Louvain Drug Research Institute (LDRI), Université Catholique de Louvain (UCLouvain), 1200, Brussels, Belgium
[d] Walloon Excellence in Life Sciences, and Biotechnology (WELBIO) Research Institute, 1300, Wavre, Belgium

ARTICLE INFO

Keywords:
EPR
ESR
Nitroxide
Mitochondria
ROS
Cancer
mitoTEMPO
3-Carbamoyl-proxyl

ABSTRACT

Because the precise site of ROS production plays a key role in cellular redox signaling and its (patho)physiological consequences, it is crucial to develop tools that enable site-specific detection of ROS in complex systems, including *in vivo*. Here, we propose the use of Electron Paramagnetic Resonance (EPR) and dual nitroxide sensors composed of mitoTEMPO and carbamoyl-proxyl (3CP) to probe ROS production in the mitochondrial and intracellular/extracellular compartments, respectively. For the proof-of-concept, the decay rates of the nitroxides were measured in 4T1 breast tumor models, both *in vitro* and *in vivo*, using 9 GHz and 1 GHz spectrometers, respectively. To modulate the level of ROS either in the cytosol or in the mitochondria, cells and mice were treated with either the glutathione synthesis inhibitor L-Buthionine Sulfoximine (L-BSO) or Antimycin A, an inhibitor of the complex III of the mitochondrial electron transport chain, or their appropriate controls. In mice, an increase in relative decay rate was observed for 3CP, but not for mitoTEMPO, 1 and 2 days after starting L-BSO treatment, while the opposite result was obtained after Antimycin A treatment. These observations were consistent with results obtained on cells *in vitro*. *Ex-vivo* analyses of tumors, with or without ferricyanide that converts hydroxylamines back to nitroxides, revealed non-significant changes in the total amount of nitroxide + hydroxylamine, suggesting that the blood wash-out did not play a role in the decay of the nitroxide signal. In addition, the use of genetically engineered 4T1 cells that overexpress the mitochondrial isoform superoxide dismutase 2 (SOD2) allowed the assessment of the contribution of superoxide production to EPR signal decay. Overall, this study identifies a new protocol to noninvasively discriminate the site of ROS production *in vivo*.

1. Introduction

The distribution of reactive oxygen species (ROS) across subcellular compartments controls specific ROS-mediated signaling pathways [1–3]. Hence, a recent consensus expert recommendation advocated for developing innovative tools that would enable site-specific ROS detection in cells and model organisms [2]. The most popular method for ROS detection and the localization of their production site is the use of redox-sensitive fluorescent dyes such as dichlorodihydrofluorescein diacetate (DCFH-DA), hydroethidine (HE) and mitoSOX (whereby HE is covalently bound to a triphenylphosphonium group for mitochondrial accumulation) [4,5]. However, these probes lack specificity regarding the species detected and therefore require the use of HPLC to discriminate between ROS adducts and self-oxidation products of the probe itself [4,6,7]. In addition, due to depth penetration issues, *in vivo* applications of these optical probes are limited. Electron paramagnetic resonance (EPR) has the potential to assess ROS production both *in vitro* and *in vivo* using spin traps or ROS scavengers. Spin traps (for example, nitrones) are stable diamagnetic species that produce paramagnetic compounds after their reaction with short-lived radicals. The stable spin adducts present an EPR spectrum that is a fingerprint of the trapped free radical [8]. However, the low yield in spin adducts formation and the instability of the adducts strongly limit the capability to detect them noninvasively. In contrast, the use of paramagnetic nitroxides offers an opportunity to

* Corresponding author. Biomedical Magnetic Resonance, Avenue Mounier 73.08, B-1200 Brussels, Belgium.
E-mail address: bernard.gallez@uclouvain.be (B. Gallez).

https://doi.org/10.1016/j.redox.2025.103871
Received 8 August 2025; Received in revised form 28 August 2025; Accepted 13 September 2025
Available online 15 September 2025

detect ROS *in vivo*. *In vivo,* nitroxide reduction results from a combination of different pathways, whose relative contributions depend on the nitroxide's physicochemical properties and subcellular localization [9]. In most tissues, **nitroxides can be reduced enzymatically via NAD(P)H-dependent oxidoreductases** or by **glutathione (GSH)-mediated enzymes** [10,11]**.** A third but significant mechanism involves **reactive oxygen species (ROS)**. Superoxide ($O_2^{\bullet-}$), in particular, can oxidize nitroxides into an **oxoammonium cation ($R_2N^+=O$)**, which is then rapidly reduced to the hydroxylamine (R_2NHOH) by intracellular NADH or NADPH:

$$\bullet R_2NO^\bullet + O_2^{\bullet-} \rightarrow R_2N^+=O$$

$$\bullet R_2N^+=O + NAD(P)H \rightarrow R_2NHOH + NAD(P)^+$$

This ROS-initiated two-step mechanism becomes especially relevant under oxidative stress [12]. The hydroxyl radical ($^\bullet OH$) reacts with nitroxides, leading to either oxoammonium cation formation or to irreversible ring modifications depending on the nitroxide's structure and local environment [13]. Although $^\bullet OH$ is highly reactive and has an extremely short half-life it can still induce the nitroxide reduction. Hydrogen peroxide (H_2O_2), in contrast, does not react directly with nitroxides under physiological conditions, but it can significantly influence their redox state through indirect mechanisms. One major pathway is the Fenton reaction, in which H_2O_2 reacts with reduced transition metals (notably Fe^{2+}) to generate hydroxyl radicals ($^\bullet OH$) [14].

When administered in a tissue, nitroxides are mainly metabolized to the corresponding hydroxylamine forms [15]. This intrinsic *in vivo* one-electron reduction of the nitroxide can be modified (amplified or delayed) by abnormal tissue redox conditions [15] such as oxidative stress conditions accompanying ROS production (Fig. 1A). Therefore, assessment of redox status *in vivo* can be achieved by monitoring EPR signal decay of the nitroxide over time using low frequency EPR spectroscopy/imaging, or by a decrease in contrast in MRI or dynamic nuclear polarization (DNP)-MRI [16–18]. So far, most studies used non targeted nitroxides to detect the redox status *in vivo* [16,19–24]. MitoTEMPO, a nitroxide that selectively accumulates in mitochondria [25,26], has been used as a redox marker *in vivo* in a few studies in models of kidney dysfunction and Parkinson's disease [27,28]. Of note, while the literature reports that hydrophilic nitroxides are reduced less efficiently by mitochondria than lipophilic nitroxides such as mitoTEMPO [29,30], the actual value of this sensor to selectively detect mitochondrial ROS has never been firmly established. Indeed, this probe has not been directly compared to nitroxides with a non-selective intracellular distribution.

One of the most important fields of application of site-specific ROS detection is oncology. In tumors, redox regulation modulates tumor initiation, proliferation, metastasis, programmed cell death, autophagy, and metabolic reprogramming [31]. Depending on the context, ROS exert paradoxical effects on cancers. At an intermediate level, ROS stimulate tumorigenesis and support the progression of cancer cells, while an excessive concentration leads to cell death [32]. The upregulated antioxidant defenses of cancer cells often limit ROS levels to a tumor-promoting level [31–36]. Because mitochondria are major producers of ROS in cells [37,38], the role of mitochondrial ROS (mtROS) has received considerable attention in cancer research over the last years [39]. The involvement of mtROS in the metastatic process [34,35] has stimulated the development of selective mtROS scavenging approaches to inhibit cell migration and invasion [40–42]. Opposingly, research has been conducted to selectively boost the level of mtROS to achieve cancer cell cytotoxicity [43–45]. In this context, it is of paramount importance to be able to titrate and identify the origin of ROS production in biological media and *in vivo*.

The present study aims to assess the value of EPR spectroscopy using a dual probe for site-specific ROS detection *in vitro* and *in vivo*. For this purpose, we compared two nitroxides showing accumulation in different cellular compartments to determine the capacity of EPR spectroscopy to discriminate the origin of ROS production within cells. We used two commercially available nitroxides, the 3-Carbamoyl Proxyl (3CP), a non-targeted hydrophilic nitroxide that distributes throughout both in extra- and intra-cellular compartments [46] and has been used for the global detection of ROS *in vivo* [16,19–21,23]. For specific mtROS detection, we used mitoTEMPO, a mitochondria-targeted nitroxide [47] (Fig. 1B). Of note, mitoTEMPO has never been used in tumors for mtROS detection, and the respective value of both compounds has not been compared in the literature. As a proof of concept, we modulated the level of ROS in the cytosol by exposing cells or mice to glutathione depletion (using L-Buthionine Sulfoximine (L-BSO)) [20,22], or in mitochondria by inhibiting the electron transport chain (using Antimycin A, an inhibitor of complex III) [48]. EPR signal decay was monitored over time in breast cancer cells *in vitro* and in breast tumors *in vivo*, using 9 GHz and 1 GHz EPR spectroscopy, respectively. Because EPR decay could be influenced by probe wash-out via perfusion [49], we also assessed the respective contribution of reduction and wash-out to EPR signal decay. Finally, we genetically modified cancer cells to over-express superoxide dismutase 2 (SOD2), the mitochondrial isoform of SOD [50], to assess the contribution of mitochondrial superoxide to the EPR signal decay.

2. Materials and methods

2.1. Superoxide production by enzymatic assay

To produce superoxide, a Xanthine/Xanthine Oxidase system was used. Xanthine (Sigma-Aldrich, Hoeilaart, Belgium) and Xanthine Oxidase (Sigma-Aldrich) were added at the concentration of 1 mM and 5 mU/ml, respectively, to PBS buffer (Thermo Scientific, pH 7.4) with 1 mM of NADH (Sigma-Aldrich) and 1 mM of diethylenetriaminepentaacetic acid (DTPA, Sigma-Aldrich). This system allows a superoxide production of 1.97 μM/min as described elsewhere [51]. The EPR probes mitoTEMPO (CAS number: 1334850-99-5, Bio-Connect, Huissen, the Netherlands) and 3-Carbamoyl-PROXYL (3CP, CAS number: 4399-80-8, Sigma-Aldrich) were added at a final concentration of 20 μM, and the mixture was transferred in a sealed hematocrit capillary and inserted into a quartz tube. Superoxide dismutase (SOD, Sigma-Aldrich) at a concentration of 200 U/ml was used as a control. The sample was placed in the EPR cavity of a Bruker EMX-Plus spectrometer operating in X-band (9.85 GHz) and equipped with a PremiumX ultra-low noise microwave bridge and a SHQ high sensitivity resonator, and an acquisition was recorded every 40 s. The EPR parameters set in Bruker Xenon Spin fit program were as follows: microwave power, 20 mW; frequency modulation, 100 kHz; modulation amplitude, 0.1 mT; center field 336.5 mT; sweep width, 1.5 mT; sweep time 30.48s. Data were analyzed by performing a double integration of the nitroxide middle peak to obtain the intensity of the signal over time.

2.2. ROS measurements on whole cells exposed to redox modulators

4T1 mouse breast cancer cells were obtained from the American Type Culture Collection (ATCC, Manassas, VA, USA) and maintained in culture in RPMI 1640 medium (Gibco, Thermo Scientific, Merelbeke, Belgium) supplemented with 10 % heat-inactivated fetal bovine serum (HI FBS, Gibco, Thermo Scientific). The day prior to acquisition, cells were treated with either 25 μM L-Buthionine Sulfoximine (L-BSO, Sigma-Aldrich), 7.5 nM or 1 μM Antimycin A (Sigma-Aldrich) or the appropriate control (PBS for the L-BSO experiments and 0.1 % DMSO for the Antimycin A experiments). On the day of acquisition, cells were harvested to obtain a solution of 25×10^6 cells/ml. A mixture was prepared with 40 μL of cell suspension, 0.5 μL DTPA (100 mM) and 7.5 μL PBS. MitoTEMPO or 3CP were added to obtain a final concentration of 20 μM. The mixture was transferred into a 12 cm long PTFA tube (inside diameter 0.025 in, wall thickness 0.002 in). The tube was folded and inserted into an open quartz tube. The sample was placed in the EPR

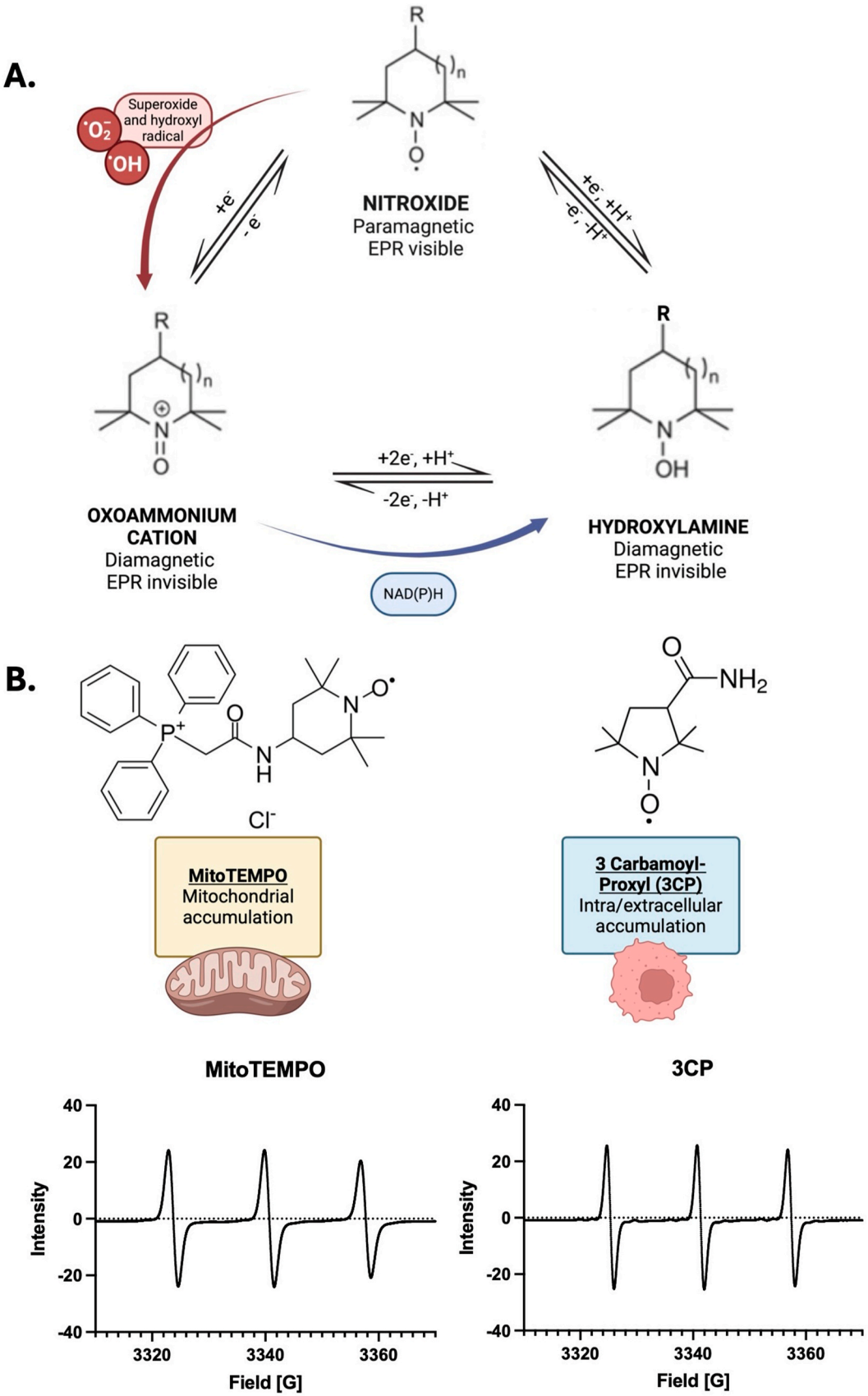

Fig. 1. Principle of the assay. (A) Redox transformation of nitroxides in tissues. *In vivo*, nitroxides can be reduced to the corresponding hydroxylamines, or they can be oxidized to an oxoammonium cation by ROS. The oxoammonium cation can be reduced back to the nitroxide by superoxide by a one-electron reduction, or to the corresponding hydroxylamine by glutathione (GSH) by a two-electrons reduction. (B) Structures of MitoTEMPO and 3CP and their respective spectra, used as sensor of ROS production in the mitochondria and intracellular/extracellular compartment, respectively.

cavity of the spectrometer heated at 37 °C with a continuous gas flow with 1 % of oxygen (concentration commonly found in tumors *in vivo*). An acquisition was launched every 40 s. The EPR parameters used were as previously described (see above section). ROS contribution in signal intensity changes was calculated as the difference between the intensity of the nitroxide peak for the last acquisition minus the intensity for the first acquisition ($\Delta T = 15$ min).

2.3. Tumor models and treatments

All experiments involving animals were allowed by the local ethics committee (UCLouvain agreement reference: 2022/UCL/MD/33) and performed in accordance with Belgian law for the protection and welfare of animals. Six weeks old females BALB/cAnNRJ (Janvier Labs, France) were housed under standardized light and temperature conditions of light and temperature (12-h daylight cycle, 22 ± 2 °C) before and during the experiments. All animals had ad libitum access to chow pellets and water. After acclimation, 2×10^5 4T1 cells were inoculated in the right hind leg muscle. Tumor sizes were monitored using an electronic caliper. Tumor shape was assumed to be ellipsoidal; hence, the volume was considered $\pi/6 \times X \times Y^2$, where X and Y are the two distances measured ($X < Y$). When tumor size reached a diameter of 7 mm ($\cong$ 250 mm^3), mice were randomly allocated to experimental groups.

Mice were treated for 3 days with either 500 mg/kg of L-BSO, 0.3 mg/kg of Antimycin A or the appropriate controls (saline solution for L-BSO experiment or DMSO for Antimycin A experiment). The treatment was injected intraperitoneally by alternating the injection site.

2.4. In vivo L-band EPR

When tumor size reached a diameter of 7 mm ($\cong$ 250 mm^3), mice were randomly allocated to four groups (n = 6/group). A first EPR acquisition was done to obtain the basal decay rates of mitoTEMPO and 3CP. Mice were anesthetized with isoflurane. The induction was performed with 3 % of isoflurane and anesthesia was maintained with 1.5 % for 15 min to avoid perturbations in hemodynamics [52]. Mouse body temperature was monitored and maintained with a warm blanket and respiration rate was monitored during the whole acquisition. Then, 25 μmol/kg of mitoTEMPO or 3CP were injected in the tumor (50 μL, multi-sites injection) and the mouse was placed in the EPR cavity with the tumor in contact with the loop surface coil resonator (Fig. S1). The nitroxide concentration has been chosen because it provides a good signal to noise ratio while keeping a short acquisition time. Two minutes after the injection, an EPR spectrum was recorded every 90 s using an EPR spectrometer (electromagnet from Magnettech, Berlin, Germany; electronic console from Clin-EPR, Lyme, NH, USA) with a low frequency microwave bridge operating at 1.1 GHz (Fig. S1). EPR parameters were as follows: power, 20 mW; frequency modulation, 100 kHz; modulation amplitude, 0.1 mT; sweep time, 5s; sweep width 0.5 mT; number of scans, 12. Nitroxides signal decay follows a one-phase exponential decay and thus, the apparent signal decay rates were determined by the following equation:

$$Decay\ rate = \frac{Ln(intensity\ T2) - Ln(intensity\ T1)}{T2 - T1}$$

where T1 and T2 are signal intensities measured after 2 min and 10 min, respectively.

After the first acquisition, mice were treated daily with either L-BSO, Antimycin A or the appropriate control. Each day, a new EPR acquisition was performed to study the evolution of nitroxides decay rates over time.

2.5. Ex-vivo analysis

On the third day of treatment with L-BSO, Antimycin A or control, an *ex-vivo* analysis was performed to measure the concentration of nitroxides and hydroxylamines in tumors. To do so, mice were anesthetized with isoflurane, as previously described. 50 μL of MitoTEMPO or 3CP (25 μmol/kg) were injected in the tumors, which were harvested 2 min (start of *in vivo* acquisition) or 10 min later and quenched in liquid nitrogen to stop metabolism. Then, the tumors were homogenized in PBS using a mechanical lyser (TissueLyser II, Qiagen, Hilden, Germany). Half of the homogenate was diluted in PBS (1:1 dilution) and the other half in a solution of ferricyanide (2 mM, 1:1 dilution) to quantitatively convert the hydroxylamine produced (due to *in vivo* reduction) back to the nitroxide form [19]. The sample was transferred into a sealed hematocrit capillary and placed in the EPR cavity. EPR parameters were as described previously. The concentration was calculated from a standard curve of mitoTEMPO or 3CP dissolved in PBS with/without ferricyanide (2 mM) (Fig. S2).

2.6. 4T1 cells transfection with SOD2

10^5 cells were seeded in a 6-well plate. Lipofectamine (Thermo Scientific, Merelbeke, Belgium) was used in antibiotic-free media to transfect a plasmid encoding SOD2 (Sino Biological, catalog # HG12061-CY, Heschborn, Germany) according to the manufacturer's protocol. Two days after, the cells were expanded to 100 mm Petri dishes. The next day, they were treated with 500 μg/ml of Hygromycin B (Sigma-Aldrich). After 10 days of incubation with Hygromycin B, single cell colonies were left to grow in antibiotic-free media. Cells were then picked, expanded and a Western blot analysis was performed to confirm SOD2 over-expression.

2.7. Western blotting

4T1 and 4T1-SOD2 cells were harvested from 100 mm Petri dishes and lysed in RIPA buffer (Sigma-Aldrich) with 1 % Halt protease inhibitors and Halt phosphatase inhibitors (ThermoFisher). For PRX1 and PRX3 immunoblotting, cysteine residues were alkylated (to determine the oxidized and reduced isoforms) and proteins extracted using a non-reducing environment as explained elsewhere [53]. 20 μg of proteins were separated by SDS-PAGE and transferred to PVDF membranes (Bio-Rad, Temse, Belgium). Membranes were incubated overnight with primary antibodies. Anti-SOD2 rabbit monoclonal antibodies (#D3X8F; Cell Signaling Technology, Leiden, The Netherlands) Anti-PRX1 rabbit monoclonal antibodies (#EPR5433, Abcam, Cambridge, United Kingdom), anti-PRX3 rabbit monoclonal antibodies (#EPR8114, Abcam) and anti-HSP90 rabbit polyclonal antibodies (#E289; Cell Signaling Technology) were diluted (1:1000) in Tris-buffered saline Tween-20 containing 1 % of dry milk. Membranes incubated 1 h at room temperature with second antibody Peroxidase AffiniPure™ Goat Anti-Rabbit IgG from Jackson IR (Ely, United Kingdom). The revelation was performed using chemiluminescent substrate SuperSignal® West Pico (ThermoScientific) and quantified with ImageQuant LAS 500 (GE Healthcare, Chicago, IL, USA). HSP90 expression levels served as a loading control.

2.8. Mitochondrial nitroxide fraction quantification

20×10^6 cells were harvested, collected in eppendorfs tubes and left incubated for 10 min with 1 mM of either 3CP or MitoTEMPO. The mitochondria were isolated using the Mitochondria Isolation Kit for Cultured Cells by Thermo Scientific following the manufacturer's instructions. The mitochondria fraction was treated with ferricyanide (2 mM, 1:1 dilution) just prior quantification to convert the hydroxylamine (due to nitroxide reduction) back to the nitroxide form. Nitroxide concentrations were measured with X-Band EPR with the same parameters as previously described. The concentration was determined from standard curves.

2.9. Statistical analysis

Statistical analysis was performed on Graph Pad Prism 9.5. All data are shown means ± SEM. The numbers of replicates and applied statistical tests are indicated in the legend of each figure.

3. Results and discussion

3.1. In vitro confirmation of site-specificity of ROS detection by the dual probe

The implementation of the new toolbox to detect global ROS and mtROS was performed by steps of increasing complexity. First, we assessed that the decay of the EPR signal coming from both probes was sensitive to the presence of ROS. An enzymatic system, xanthine/xanthine oxidase, was first used as it is well known to produce superoxide radical in the presence of oxygen and NADH (Fig. 2A) [54]. DTPA (1 mM) was added to the system to prevent unwanted Fenton's reaction. Superoxide produced by the enzymatic reaction reacted with the nitroxides leading to a decrease in the EPR signal intensity over time with a stabilization of the signal after 10 min probably due to the inhibition of XO by its product, the uric acid (Fig. 2B–E) [55,56]. To confirm that the decay was well due to the presence of superoxide, SOD was added to the mixture in control experiments. SOD consumed superoxide before it reacted with the nitroxides and countered changes in EPR signals (Fig. 2B and C).

Then, we tested the ability of the method to detect redox modulation in different compartments of cells. We hypothesized that mitoTEMPO is more sensitive than 3CP to mitochondrial redox modulations. This is thought to be due primarily to the better penetration and greater accumulation of mitoTEMPO in mitochondrial lipid membranes. Our results support this hypothesis, showing that mitoTEMPO accumulates more efficiently in mitochondria than 3CP (Fig. S3). Of note, the difference in mitochondrial accumulation between MitoTEMPO and 3CP is not as pronounced as reported in the literature. This may be due to the high nitroxide concentration required to achieve a signal above the EPR detection limit after mitochondrial isolation.

To assess the sensitivity of the two nitroxides for redox modulation in different cellular compartments, 4T1 cells were exposed to either L-BSO, an agent inducing glutathione depletion [20,22], or Antimycin A, an inhibitor of mitochondrial complex III (increasing superoxide production) [48], leading to ROS production in the cytosol and the mitochondria, respectively. We verified the compartmentalization of ROS production induced by L-BSO and Antimycin A using immunoblot analysis of Peroxiredoxins 1 (PRX1, cytosolic isoform) and 3 (PRX3, mitochondrial isoform). Upon hydrogen peroxide exposure, PRX1 and PRX3 become oxidized and form dimers, marker of localized oxidative stress [53]. Treatment with L-BSO led to a decrease in intracellular glutathione levels and a reduced GSH/GSSG ratio, consistent with an increase in oxidative stress (Fig. S4A). This stress was predominantly cytosolic, as indicated by the accumulation of oxidized PRX1 without significant changes in PRX3 oxidation (Fig. S4B). In contrast, treatment with low-dose Antimycin A triggered mitochondrial ROS production, as evidenced by the selective oxidation of PRX3 (Fig. S4C). MitoTEMPO

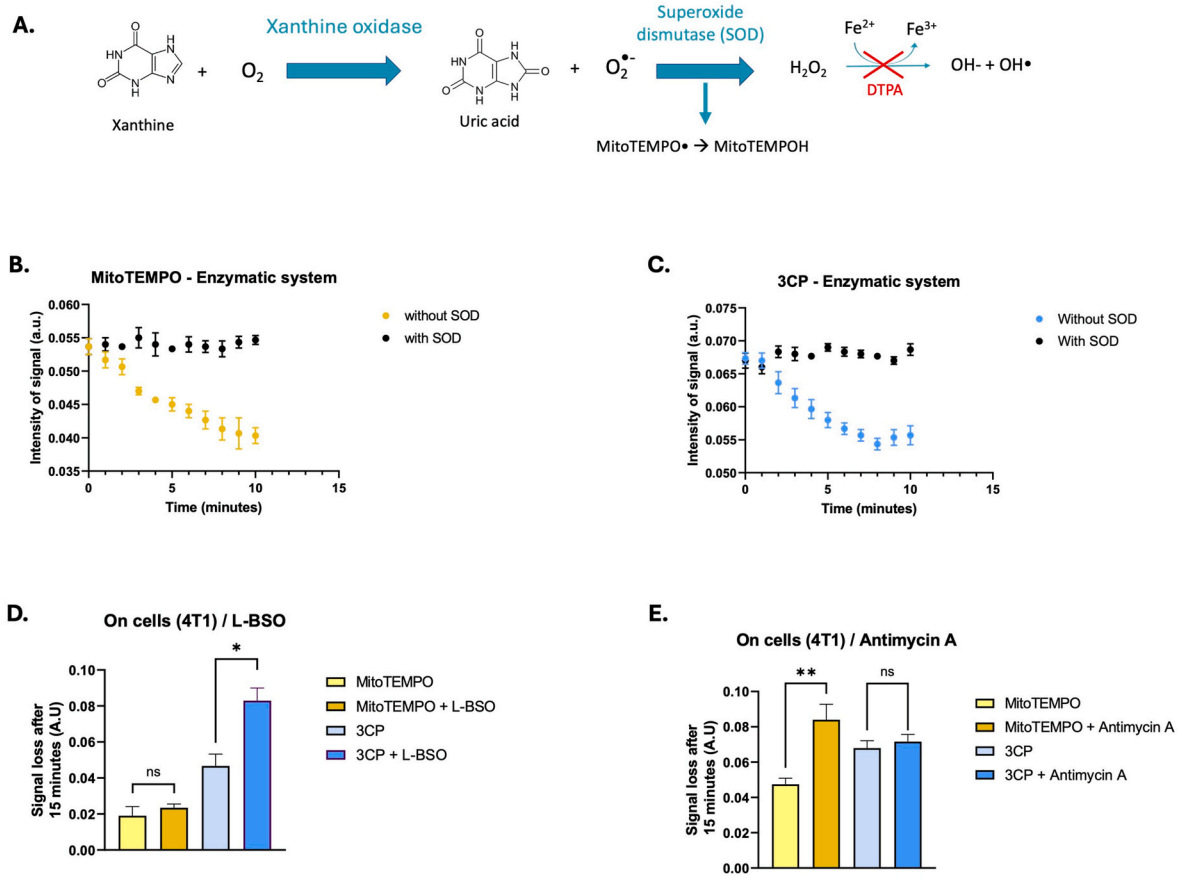

Fig. 2. *In vitro* characterization of nitroxide signal decay. (A) Xanthine (1 mM)/Xanthine (5mU/ml) oxidase system used to produce superoxide (1.97 μM/min). (B) MitoTEMPO (20 μM) signal decay when superoxide was produced by the enzymatic system. Points represent means ± SEM, n = 3. (C) 3CP (20 μM) signal decay when superoxide was produced by the enzymatic system. Points represent means ± SEM, n = 3. (D) Signal loss after 15 min when the cells were exposed to 25 μM of L-BSO or PBS (control) for 24 h. Bars represent mean ± SEM. n = 3 with 3 technical replicates, Nested one-way ANOVA, *; $p < 0.05$. (E) Signal loss after 15 min when the cells were exposed to 7.5 nM of Antimycin A or 0.1 % DMSO (control) for 24 h. Bars represent mean ± SEM. n = 3 with 3 technical replicates, one-way ANOVA, **; $p < 0.01$.

and 3CP were added at a concentration of 20 μM on cells pretreated previously for 24 h with either L-BSO or Antimycin A and EPR spectra were recorded every 40 s for 15 min (Fig. S5). L-BSO (25 μM) induced significant EPR signal loss after 15 min for 3CP, but not for mitoTEMPO$^{\bullet}$ (Fig. 2D). In contrast, Antimycin A (7.5 nM) led to a significant signal loss for mitoTEMPO$^{\bullet}$, but not for 3CP (Fig. 2E). Overall, these results demonstrate the capability of the assay to detect redox stress induced in different compartments of the cells. Of note, when used at high concentration (1 μM), Antimycin A induced a significant signal loss for both 3CP and mitoTEMPO, likely due to a massive production of ROS that may diffuse outside the mitochondria (Fig. S4D).

3.2. Noninvasive site-specificity of ROS detection in tumors in vivo by the dual probe

For *in vivo* assays in 4T1 tumor-bearing mice, the basal kinetics of EPR signal decay (without treatment) was first assessed in tumors with L-Band (1 GHz) EPR spectroscopy. The signal intensity of both 3CP and mitoTEMPO decreased monoexponentially (Fig. S6). To evaluate the specificity of this method to differentiate cytosolic *versus* mitochondrial ROS levels in tumors, the decay rates were daily measured for each probe in mice that were treated with either L-BSO (500 mg/kg per day) or Antimycin A (0.3 mg/kg per day). The mitoTEMPO decay rate was not significantly affected by L-BSO treatment that modulates ROS level in the cytosol (Fig. 3A–E) but was significantly increased after Antimycin A treatment that increases mtROS production (Fig. 3B–F). In sharp contrast, the decay rate of 3CP significantly increased after L-BSO treatment (Fig. 3C–E), while Antimycin A did not significantly alter the decay rate of this probe (Fig. 3D–F). There were no differences in tumor sizes between the groups, and the signal decay rates were not correlated with tumor sizes (Fig. S5). These results demonstrated the ability to discriminate between different sites of ROS production noninvasively in tumors *in vivo*. The results not only recapitulated the results obtained *in vitro* (Fig. 2D and E), but they also extended the applicability to *in vivo* situations in tumors using low-frequency EPR spectroscopy.

3.3. Blood wash-out did not contribute significantly to the EPR signal decay

While the previous results showed that L-BSO and Antimycin A induced differing consequences on nitroxide decay kinetics, it was important to check that this was due to different sites of ROS production while removing confounding factors bias. For example, it has been described that changes in perfusion/hemodynamics could play a role in

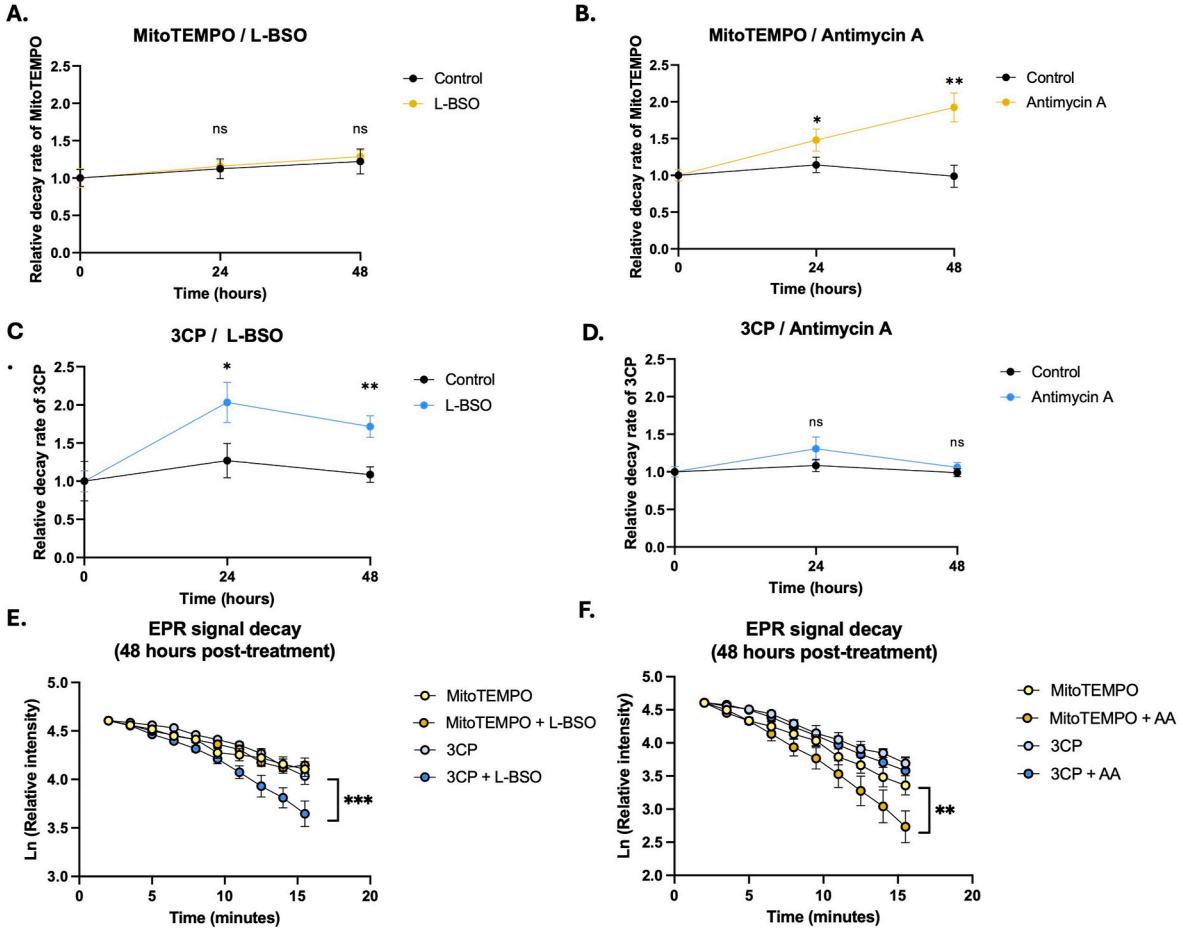

Fig. 3. *In vivo* decay rates of nitroxides over time when mice were treated with different redox modulators. (A) Decay rate over time of MitoTEMPO (25 μmol/kg) when mice were treated ± 500 mg/kg of L-BSO. All data are shown as means ± SEM. n = 6/group, one tailed paired *t*-test. ns = non significant (B) Decay rate over time of MitoTEMPO (25 μmol/kg) when mice were treated with 0.3 mg/kg of Antimycin A. All data are shown as means ± SEM. n = 6/group, one tailed paired *t*-test, *; $p < 0.05$, **; $p < 0.01$. (C) Decay rate over time of 3CP (25 μmol/kg) when mice were treated with 500 mg/kg of L-BSO. All data are shown as means ± SEM. n = 6/group, one tailed paired *t*-test, *; $p < 0.05$, **; $p < 0.01$. (D) Decay rate over time of 3CP (25 μmol/kg) when mice are treated with 0.3 mg/kg of Antimycin A. All data are shown as means ± SEM. n = 6/group, one tailed paired *t*-test. (E) Signal decay over time for mitoTEMPO and 3CP (25 μmol/kg) when mice were treated with 500 mg/kg of L-BSO for 48 h. All data are shown as means ± SEM. n = 6/group, two-way ANOVA, ***; $p < 0.005$. (F) Signal decay over time for mitoTEMPO and 3CP (25 μmol/kg) when mice were treated with 0.3 mg/kg ofAntimycin A (AA). All data are shown as means ± SEM. n = 6/group, two-way ANOVA, **; $p < 0.01$.

the wash-out of nitroxides [49]. Therefore, we elucidated the respective contribution of nitroxide reduction by ROS and wash-out to EPR signal decay. To assess this, the tumors were harvested 2 min or 10 min after nitroxide injection and quenched in liquid nitrogen to stop further reactions. The respective ratios of nitroxides and hydroxylamines were quantified by reconstitution in a ferricyanide solution that quantitatively converts produced hydroxylamines *in vivo* back to their nitroxide forms [19]. Concentrations of the different forms, "nitroxide alone" and "nitroxide + hydroxylamine", measured in the different groups of mice are presented in the top and bottom of Fig. 4, respectively. These *ex-vivo* quantifications of nitroxide (Fig. 4, top) confirmed the changes observed *in vivo*. A first observation was that, after L-BSO treatment, the nitroxide form of 3CP significantly decreased compared to the untreated group, while the decay of mitoTEMPO (nitroxide form) was not significantly different from the control group (Fig. 4 A). Conversely, after Antimycin A treatment, 3CP (nitroxide form) did not significantly decrease compared to the untreated group, while the decay of mitoTEMPO was significantly more pronounced compared to the control group (Fig. 4B). Most importantly, when measuring the combined forms (nitroxides + hydroxylamines, Fig. 4C), there was no significant change of the total content over time (2–10 min after injection) in all groups of mice. This meant that the concentrations of the probes remained stable over this short period of time, establishing that wash-out through tissue perfusion did not significantly contribute to the decay of the signals of the nitroxides, that were mainly due to their reduction in hydroxylamines. We also established that the kinetics were independent on the tumor size (Fig. S7).

3.4. Superoxide contributes partially to signal decay rate

Because superoxide is the primary ROS produced by mitochondria [37], we explored its contribution to nitroxide EPR signal decay. To establish this, a plasmid encoding SOD2 (the mitochondrial isoform of superoxide dismutase [35,50]) was transfected in 4T1 cells. SOD2 overexpression was confirmed by Western blot analyses during several passages (passage 1 to 6), as shown in Fig. 5A. Of note, we observed that the expression of SOD2 induced by transfection increased by about 40 %. As shown in Fig. 5B and C, the relative decay rate of mitoTEMPO was significantly lower in tumors produced in mice using cells overexpressing SOD2 compared to wild-type cells, while there was no significant change for the 3CP decay rate (Fig. 5B and C). These results established that mitochondrial superoxide contributed at least in part to the ROS-dependent decay rate of mitoTEMPO. Of note, while superoxide plays a significant role in the redox-dependent reduction of the nitroxide, it is unlikely that it is the sole factor contributing to the EPR signal decay as, *in vitro*, overexpression of SOD2 did not fully abrogate the decrease in EPR signal (Fig. S8). It is likely that nitroxides do not only react with superoxide but also with other ROS, such as hydroxyl radical and/or reactive nitrogen species (RNS). It is also established in literature that lipophilic nitroxides such as mitoTEMPO can be reduced *in vivo* by mitochondria ETC and thus the use of appropriate controls (such as SOD) is required to differentiate the contribution of superoxide or complex III in nitroxide bioreduction [29,57]. It is also noteworthy that *in vivo* decay rates were measured over the whole tumor region, meaning that our method is not capable of distinguishing between the different types of cells present in the tumor microenvironment (cancer cells, cancer associated fibroblasts, immune cells, …) [58,59]. When we compared tumors formed from wild-type cancer cells to tumor formed from cancer cells overexpressing SOD2, it is likely that cancer cells represented only a fraction of all the cells contributing to the reduction of the nitroxides in tumors.

Overall, one of the main strengths of this assay resides in the fact that

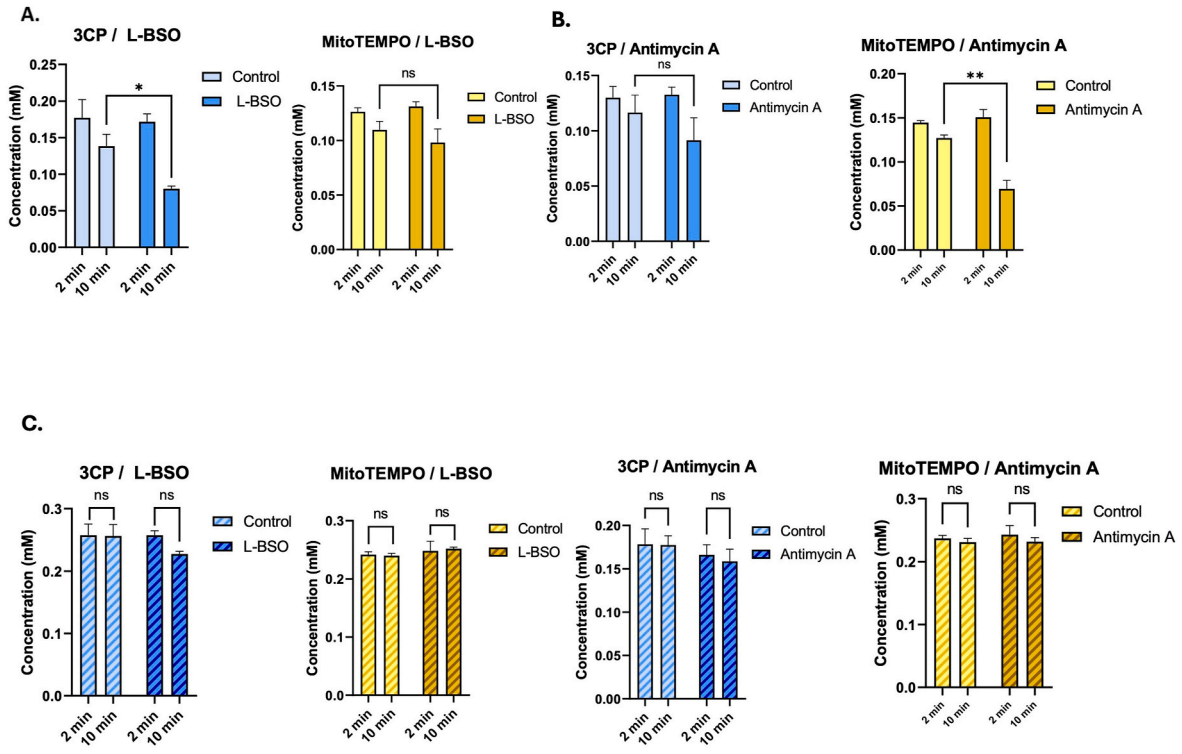

Fig. 4. Evolution of the concentration of the nitroxide form (top) and of the combined forms (nitroxide + hydroxylamine) (bottom) of 3CP and MitoTEMPO$^{\bullet}$ in tumors over time. (A) Nitroxide concentration after 2 or 10 min when mice were treated ± 500 mg/kg of L-BSO. Bars represent mean ± SEM. n = 3/group, two-way ANOVA with Sidak's correction, *; $p < 0.05$, ns; $p > 0.05$. (B) Nitroxide concentration after 2 or 10 min when mice were treated ± 0.3 mg/kg of Antimycin A. Bars represent mean ± SEM. n = 3/group, two-way ANOVA with Sidak's correction, **; $p < 0.01$, ns; $p > 0.05$. (C) Total product concentration (nitroxide + hydroxylamine) after 2 or 10 min when mice were treated ± 500 mg/kg of L-BSO or 0.3 mg/kg of Antimycin A. Bars represent mean ± SEM. n = 3/group, two-way ANOVA with Sidak's correction, ns; $p > 0.05$.

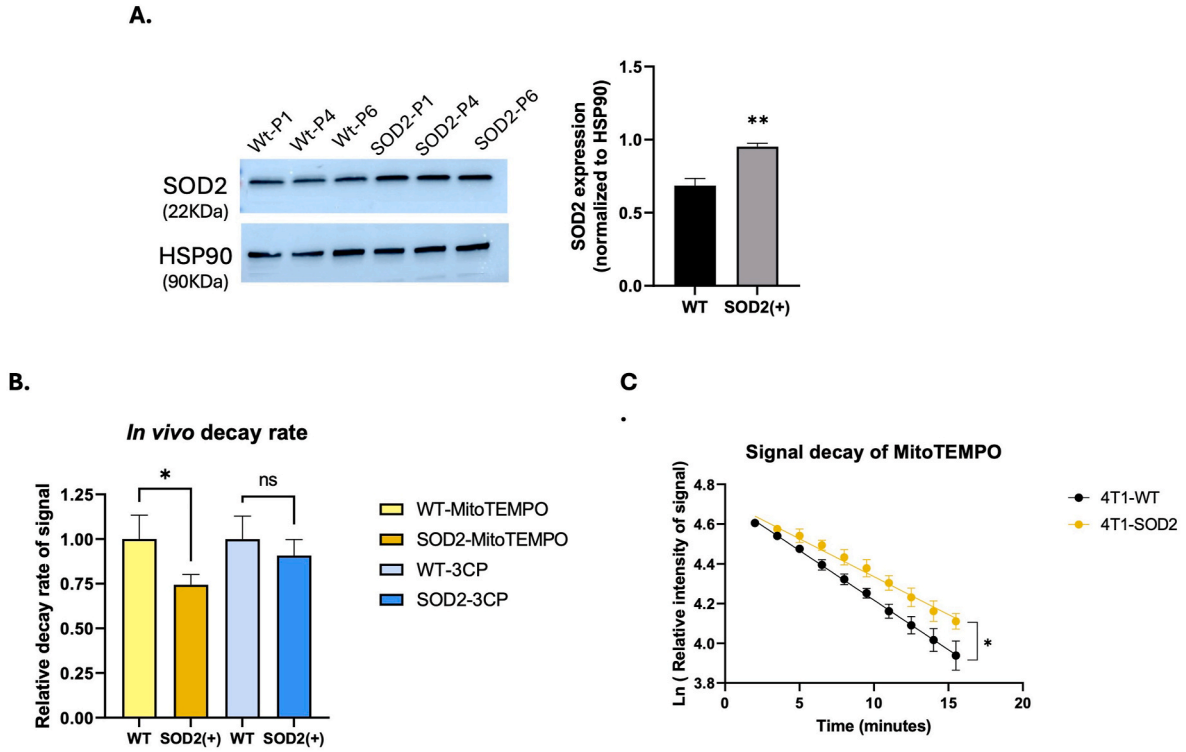

Fig. 5. Contribution of superoxide to the EPR signal decay rate in *vivo*. (A) Western blot of expression of SOD2 in wild-type 4T1 breast cancer cell and 4T1 cells transfected with a plasmid encoding SOD 2, after passages 1, 4 and 6. Student's t-test, n = 3, **; $p < 0.01$ (B) Decay rates of nitroxides *in vivo* for 4T1-SOD2 tumors compared to wild-type 4T1 tumors. Bars represent means ± SEM. n = 6/group, Student's t-test, *; $p < 0.05$. (C) EPR signal decay of MitoTEMPO (25 μmol/kg) *in vivo*. Points represent means ± SEM. n = 6/group, two-way ANOVA with Sidak's correction, *; $p < 0.05$.

EPR spectroscopy allows for noninvasive *in vivo* ROS detection with the capacity to distinguish between the origins of ROS. This method is a promising pre-clinical tool to study redox metabolism in tumors and to analyze the role of different factors or treatments addressing different subcellular compartments. The main limitation of this assay is that it does not allow to distinguish specific ROS species originating from a same location. *In vitro*, the identification of ROS responsible for probe oxidation is possible thanks to scavengers of a given ROS [54]. *In vivo*, these controls are difficult to apply. Here, we used genetically modified models to assess the contribution of superoxide. However, as previously discussed, the use of these models does not exclude that nonmalignant cells within solid tumors also contribute to the redox state of the probes.

It is important to note that the reduction of nitroxides in biological systems is shaped by the complex interplay between cellular oxidants and the reductive capacity of each cell type. Rather than following a single, universal mechanism, nitroxide bioreduction depends on the relative abundance and activity of intracellular reductants such as GSH, NADH, NADPH, as well as redox enzymatic systems whose expression and activity vary across cell types [10,11]. The contribution of each pathway can shift dynamically in response to oxidative stress or metabolic perturbations. These considerations highlight the importance of accounting for the reductive and enzymatic landscape of each cellular model when interpreting nitroxide-based redox measurements [6].

For the future, it would be interesting to use the combination of the two probes with imaging modalities, such as EPR imaging, MRI or DNP-MRI, to further investigate the heterogeneity of the redox response of cancer cells to treatments.

CRediT authorship contribution statement

Barbara Mathieu: Writing – review & editing, Writing – original draft, Visualization, Validation, Methodology, Investigation, Formal analysis, Data curation, Conceptualization. **Justin D. Rondeau:** Writing – review & editing, Investigation, Formal analysis. **Lionel Mignion:** Writing – review & editing, Methodology, Investigation. **Pierre Sonveaux:** Writing – review & editing, Validation, Supervision, Resources, Project administration, Methodology, Funding acquisition. **Bernard Gallez:** Writing – review & editing, Writing – original draft, Validation, Supervision, Resources, Project administration, Methodology, Funding acquisition, Conceptualization.

Declaration of competing interest

P.S. is inventor of patent application WO2022/243541 "Molecular signature for assessing the responsiveness of cancer to mitochondria-targeted antioxidants". The authors declare that they have no other conflict of interest related to the present study. The sponsors had no role in study design, in the collection, analysis or interpretation of data, and in the writing of the report.

Acknowledgments

This research was supported by the Actions de Recherche Concertées program of the Communauté Française de Belgique (ARC 21/26–118), the FRFS-WELBIO strategic axis of the Walloon Region of Belgium (WELBIO-CR-2022A-13), and the Fonds National de la Recherche Scientifique (F.R.S.-FNRS) – CDR J.0084.22 and CDR J.0135.18. Barbara Mathieu is a F.R.S.-FNRS PhD Research Fellow. Justin D. Rondeau is an early-stage Researcher of EU Horizon2020 Marie Skłodowska-Curie Innovative Training Networks (ITN-ETN) grant #860245 (THERADNET). Pierre Sonveaux is a F.R.S.-FNRS Research Director and a WELBIO Research Investigator. This study used the equipment of the Nuclear and Electron Spin Technologies platform of the UCLouvain.

Appendix A. Supplementary data

Supplementary data to this article can be found online at https://doi.org/10.1016/j.redox.2025.103871.

Data availability

Data will be made available on request.

References

[1] H. Sies, D.P. Jones, Reactive oxygen species (ROS) as pleiotropic physiological signalling agents, Nat. Rev. Mol. Cell Biol. 21 (2020) 363–383.
[2] H. Sies, V.V. Belousov, N.S. Chandel, et al., Defining roles of specific reactive oxygen species (ROS) in cell biology and physiology, Nat. Rev. Mol. Cell Biol. 23 (2022) 499–515.
[3] H. Sies, R.J. Mailloux, U. Jakob, Fundamentals of redox regulation in biology, Nat. Rev. Mol. Cell Biol. (2024), https://doi.org/10.1038/s41580-024-00730-2.
[4] M. Hardy, J. Zielonka, H. Karoui, et al., Detection and characterization of reactive oxygen and nitrogen species in biological systems by monitoring species-specific products, Antioxidants Redox Signal. 28 (2018) 1416–1432.
[5] B. Kalyanaraman, G. Cheng, M. Hardy, et al., Teaching the basics of reactive oxygen species and their relevance to cancer biology: mitochondrial reactive oxygen species detection, redox signaling, and targeted therapies, Redox Biol. 15 (2018) 347–362.
[6] M.P. Murphy, H. Bayir, V. Belousov, et al., Guidelines for measuring reactive oxygen species and oxidative damage in cells and in vivo, Nat. Metab. 4 (2022) 651–662.
[7] G. Cheng, M. Zielonka, B. Dranka, et al., Detection of mitochondria-generated reactive oxygen species in cells using multiple probes and methods: potentials, pitfalls, and the future, J. Biol. Chem. 293 (2018) 10363–10380.
[8] M.J. Davies, Detection and characterisation of radicals using electron paramagnetic resonance (EPR) spin trapping and related methods, Methods 109 (2016) 21–30.
[9] N. Kocherginsky, H.M. Swartz, M. Sentjurc, Nitroxide Spin Labels: Reactions in Biology and Chemistry, CRC Press, Boca Raton, Fla, 1995.
[10] M. Davis R, B. Mitchell J, C. Krishna M, Nitroxides as cancer imaging agents, Anti Cancer Agents Med. Chem. 11 (2011) 347–358.
[11] A.A. Bobko, I.A. Kirilyuk, I.A. Grigor'ev, et al., Reversible reduction of nitroxides to hydroxylamines: roles for ascorbate and glutathione, Free Radic. Biol. Med. 42 (2007) 404–412.
[12] M.C. Krishna, D.A. Grahame, A. Samuni, et al., Oxoammonium cation intermediate in the nitroxide-catalyzed dismutation of superoxide, Proc. Natl. Acad. Sci. 89 (1992) 5537–5541.
[13] A. Samuni, S. Goldstein, A. Russo, et al., Kinetics and mechanism of hydroxyl radical and OH-Adduct radical reactions with nitroxides and with their hydroxylamines, J. Am. Chem. Soc. 124 (2002) 8719–8724.
[14] C.C. Winterbourn, Toxicity of iron and hydrogen peroxide: the fenton reaction, Toxicol. Lett. 82–83 (1995) 969–974.
[15] H.M. Swartz, N. Khan, V.V. Khramtsov, Use of electron paramagnetic resonance spectroscopy to evaluate the redox state in vivo, Antioxidants Redox Signal. 9 (2007) 1757–1772.
[16] K. Matsumoto, J.B. Mitchell, M.C. Krishna, Comparative studies with EPR and MRI on the *In vivo* tissue redox status estimation using redox-sensitive nitroxyl probes: influence of the choice of the region of interest, Free Radic. Res. 52 (2018) 248–255.
[17] T. Uchida, H. Togashi, Y. Kuroda, et al., *In vivo* analysis of redox status in organs – from bench to bedside, Free Radic. Res. 54 (2020) 961–968.
[18] F. Hyodo, H. Eto, T. Naganuma, et al., *In Vivo* dynamic nuclear polarization magnetic resonance imaging for the evaluation of redox-related diseases and theranostics, Antioxidants Redox Signal. 36 (2022) 172–184.
[19] K. Matsumoto, F. Hyodo, A. Matsumoto, et al., High-resolution mapping of tumor redox status by magnetic resonance imaging using nitroxides as redox-sensitive contrast agents, Clin. Cancer Res. 12 (2006) 2455–2462.
[20] P. Kuppusamy, H. Li, G. Ilangovan, et al., Noninvasive imaging of tumor redox status and its modification by tissue glutathione levels, Cancer Res. 62 (2002) 307–312.
[21] K. Kimura, N. Iguchi, H. Nakano, et al., Redox-sensitive mapping of a mouse tumor model using sparse projection sampling of electron paramagnetic resonance, Antioxidants Redox Signal. 36 (2022) 57–69.
[22] J. Kengen, J.-P. Deglasse, M.-A. Neveu, et al., Biomarkers of tumour redox status in response to modulations of glutathione and thioredoxin antioxidant pathways, Free Radic. Res. 52 (2018) 256–266.
[23] MdZ. Hosain, F. Hyodo, T. Mori, et al., Development of a novel molecular probe for the detection of liver mitochondrial redox metabolism, Sci. Rep. 10 (2020) 16489.
[24] F. Hyodo, K. Matsumoto, A. Matsumoto, et al., Probing the intracellular redox status of tumors with magnetic resonance imaging and redox-sensitive contrast agents, Cancer Res. 66 (2006) 9921–9928.
[25] J. Zielonka, J. Joseph, A. Sikora, et al., Mitochondria-targeted triphenylphosphonium-based compounds: syntheses, mechanisms of action, and therapeutic and diagnostic applications, Chem. Rev. 117 (2017) 10043–10120.
[26] M.P. Murphy, R.A.J. Smith, Targeting antioxidants to mitochondria by conjugation to lipophilic cations, Annu. Rev. Pharmacol. Toxicol. 47 (2007) 629–656.
[27] D. Lazarova, S. Shibata, I. Ishii, et al., Nitroxide-enhanced magnetic resonance imaging of kidney dysfunction in vivo based on redox-imbalance and oxidative stress, Gen. Physiol. Biophys. 38 (2019) 191–204.
[28] Z. Zhelev, R. Bakalova, I. Aoki, et al., Imaging of superoxide generation in the dopaminergic area of the brain in parkinson's disease, using Mito-TEMPO, ACS Chem. Neurosci. 4 (2013) 1439–1445.
[29] K. Chen, P.D. Morse, H.M. Swartz, Kinetics of enzyme-mediated reduction of lipid soluble nitroxide spin labels by living cells, Biochim Biophys Acta BBA - Biomembr 943 (1988) 477–484.
[30] H.M. Swartz, M. Sentjurc, P.D. Morse, Cellular metabolism of water-soluble nitroxides: effect on rate of reduction of cell/nitroxide ratio, oxygen concentrations and permeability of nitroxides, Biochim Biophys Acta BBA - Mol Cell Res 888 (1986) 82–90.
[31] F. Xing, Q. Hu, Y. Qin, et al., The relationship of redox with hallmarks of cancer: the importance of homeostasis and context, Front. Oncol. 12 (2022) 862743.
[32] S. Galadari, A. Rahman, S. Pallichankandy, et al., Reactive oxygen species and cancer paradox: to promote or to suppress? Free Radic. Biol. Med. 104 (2017) 144–164.
[33] S. Arfin, N.K. Jha, S.K. Jha, et al., Oxidative stress in cancer cell metabolism, Antioxidants 10 (2021) 642.
[34] P.E. Porporato, V.L. Payen, J. Pérez-Escuredo, et al., A mitochondrial switch promotes tumor metastasis, Cell Rep. 8 (2014) 754–766.
[35] S. Scheinok, T. Capeloa, P.E. Porporato, et al., An EPR study using cyclic hydroxylamines to assess the level of mitochondrial ROS in superinvasive cancer cells, Cell Biochem. Biophys. 78 (2020) 249–254.
[36] L. Tang, F. Wei, Y. Wu, et al., Role of metabolism in cancer cell radioresistance and radiosensitization methods, J. Exp. Clin. Cancer Res. 37 (2018) 87.
[37] M.P. Murphy, How mitochondria produce reactive oxygen species, Biochem. J. 417 (2009) 1–13.
[38] V. Purohit, D.M. Simeone, C.A. Lyssiotis, Metabolic regulation of redox balance in cancer, Cancers 11 (2019) 955.
[39] V.L. Payen, L.X. Zampieri, P.E. Porporato, et al., Pro- and antitumor effects of mitochondrial reactive oxygen species, Cancer Metastasis Rev. 38 (2019) 189–203.
[40] T. Capeloa, J. Krzystyniak, D. d'Hose, et al., MitoQ inhibits human breast cancer cell migration, invasion and clonogenicity, Cancers 14 (2022) 1516.
[41] T. Capeloa, J. Krzystyniak, A.C. Rodriguez, et al., MitoQ prevents human breast cancer recurrence and lung metastasis in mice, Cancers 14 (2022) 1488.
[42] T. Capeloa, J.A. Van De Velde, D. d'Hose, et al., Inhibition of mitochondrial redox signaling with MitoQ prevents metastasis of human pancreatic cancer in mice, Cancers 14 (2022) 4918.
[43] G. Cheng, J. Zielonka, O. Ouari, et al., Mitochondria-targeted analogues of metformin exhibit enhanced antiproliferative and radiosensitizing effects in pancreatic cancer cells, Cancer Res. 76 (2016) 3904–3915.
[44] G. Cheng, M. Hardy, P. Topchyan, et al., Mitochondria-targeted hydroxyurea inhibits OXPHOS and induces antiproliferative and immunomodulatory effects, iScience 24 (2021) 102673.
[45] J. Pan, Y. Lee, G. Cheng, et al., Mitochondria-targeted honokiol confers a striking inhibitory effect on lung cancer via inhibiting complex I activity, iScience 3 (2018) 192–207.
[46] S.I. Dikalov, A.E. Dikalova, D.A. Morozov, et al., Cellular accumulation and antioxidant activity of acetoxymethoxycarbonyl pyrrolidine nitroxides, Free Radic. Res. 52 (2018) 339–350.
[47] A.E. Dikalova, A.T. Bikineyeva, K. Budzyn, et al., Therapeutic targeting of mitochondrial superoxide in hypertension, Circ. Res. 107 (2010) 106–116.
[48] C.L. Quinlan, A.A. Gerencser, J.R. Treberg, et al., The mechanism of superoxide production by the antimycin-inhibited mitochondrial Q-cycle, J. Biol. Chem. 286 (2011) 31361–31372.
[49] B. Gallez, G. Bacic, F. Goda, et al., Use of nitroxides for assessing perfusion, oxygenation, and viability of tissues: *in Vivo* EPR and MRI studies, Magn. Reson. Med. 35 (1996) 97–106.
[50] I.N. Zelko, T.J. Mariani, R.J. Folz, Superoxide dismutase multigene family: a comparison of the CuZn-SOD (SOD1), Mn-SOD (SOD2), and EC-SOD (SOD3) gene structures, evolution, and expression, Free Radic. Biol. Med. 33 (2002) 337–349.
[51] S. Scheinok, P. Leveque, P. Sonveaux, et al., Comparison of different methods for measuring the superoxide radical by EPR spectroscopy in buffer, cell lysates and cells, Free Radic. Res. 52 (2018) 1182–1196.
[52] C. Baudelet, B. Gallez, Effect of anesthesia on the signal intensity in tumors using BOLD-MRI: comparison with flow measurements by laser doppler flowmetry and oxygen measurements by luminescence-based probes, Magn. Reson. Imaging 22 (2004) 905–912.
[53] A.G. Cox, C.C. Winterbourn, M.B. Hampton, Measuring the redox state of cellular peroxiredoxins by immunoblotting, in: Methods in Enzymology 474, Elsevier, 2010, pp. 51–66.
[54] D. d'Hose, P. Danhier, H. Northshield, et al., A versatile EPR toolbox for the simultaneous measurement of oxygen consumption and superoxide production, Redox Biol. 40 (2021) 101852.
[55] R. Radi, S. Tan, E. Prodanov, et al., Inhibition of xanthine oxidase by uric acid and its influence on superoxide radical production, Biochim Biophys Acta BBA - Protein Struct Mol Enzymol 1122 (1992) 178–182.
[56] S. Tan, R. Radi, F. Gaudier, et al., Physiologic levels of uric acid inhibit xanthine oxidase in human plasma, Pediatr. Res. 34 (1993) 303–307.

[57] J. Trnka, F.H. Blaikie, R.A.J. Smith, et al., A mitochondria-targeted nitroxide is reduced to its hydroxylamine by ubiquinol in mitochondria, Free Radic. Biol. Med. 44 (2008) 1406–1419.
[58] F. Weinberg, N. Ramnath, D. Nagrath, Reactive oxygen species in the tumor microenvironment: an overview, Cancers 11 (2019) 1191.
[59] S.A. DuPré, D. Redelman, K.W. Hunter, The mouse mammary carcinoma 4T1: characterization of the cellular landscape of primary tumours and metastatic tumour foci, Int. J. Exp. Pathol. 88 (2007) 351–360.

Noninvasive discrimination between mitochondrial ROS and global ROS production in solid tumors using EPR spectroscopy

Barbara Mathieu, Justin D. Rondeau, Lionel Mignion, Pierre Sonveaux and Bernard Gallez

Supplementary figures

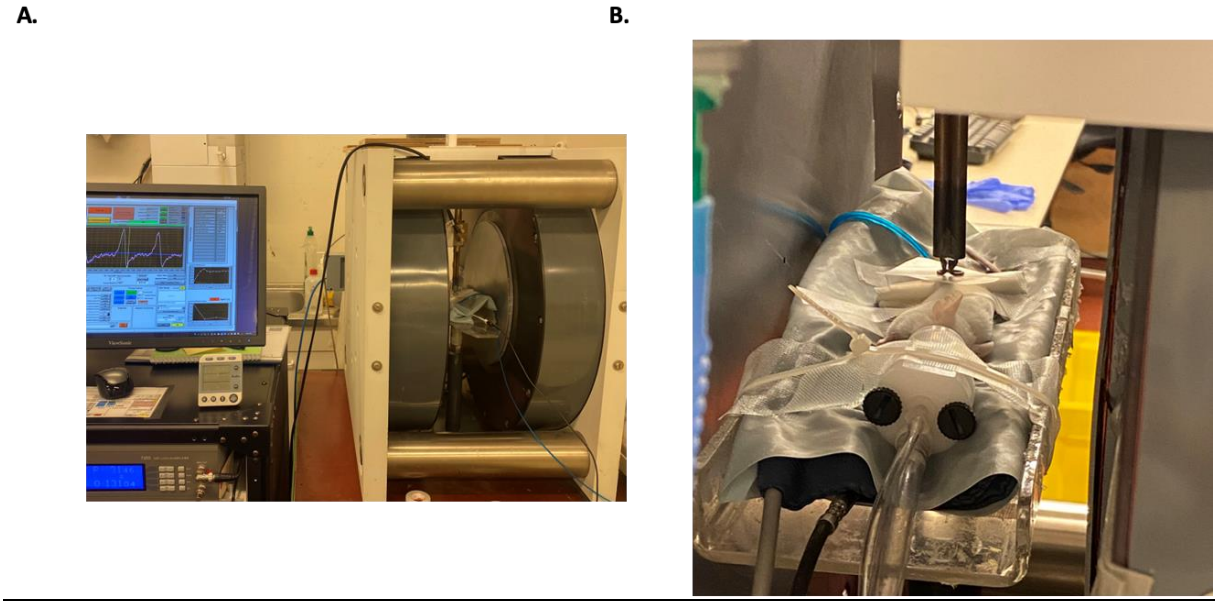

Figure S1. Experimental set-up used for *in vivo* EPR spectroscopy.
(A): EPR spectrometer with an electromagnet from Magnettech and an electronic console from Clin-EPR.
(B): Mouse anesthetized with isoflurane. The body temperature was monitored and maintained with a warm blanket. The respiration rate was monitored during the whole acquisition. A loop-gap surface coil resonator is positioned over the tumor for EPR signal monitoring.

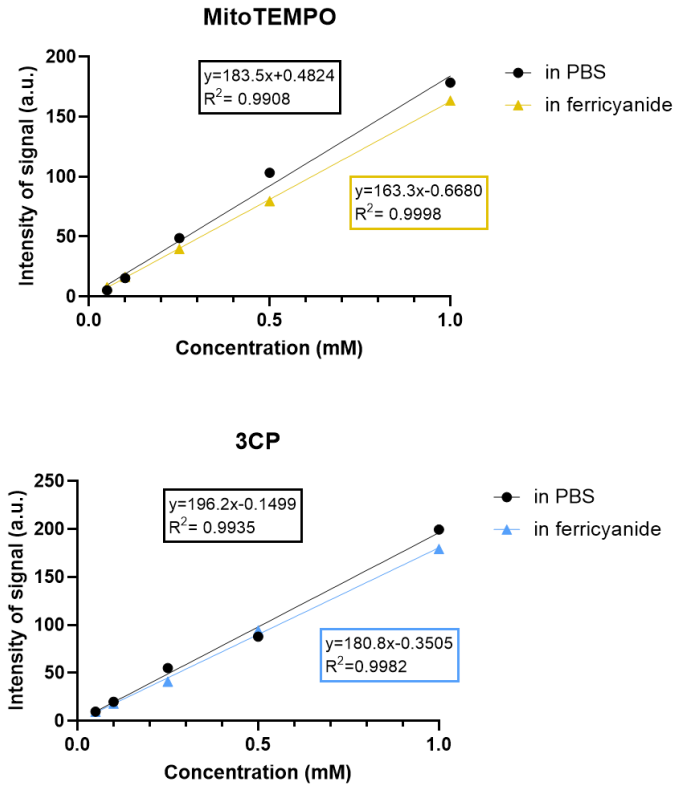

Figure S2. Calibration curves of nitroxides for *ex-vivo* analyses.
The concentration was calculated from a standard curve of MitoTEMPO• or 3CP dissolved in PBS ± ferricyanide (2 mM)

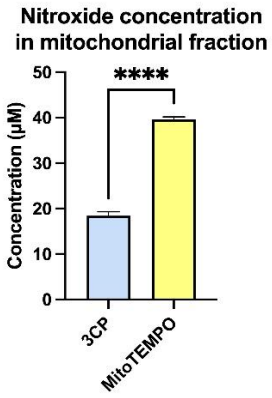

Figure S3. Concentration of 3CP and mitoTEMPO in mitochondrial fraction of 4T1 cells. Cells were incubated for 10 minutes with either 1mM of 3CP or MitoTEMPO before mitochondria isolation and treatment with ferricyanide (2mM). Concentrations were determined from calibration curves using X-Band EPR spectrometer. Bars represent mean ± SEM. n = 3 with 3 technical replicates, Student's T-test, ****; $p < 0.001$

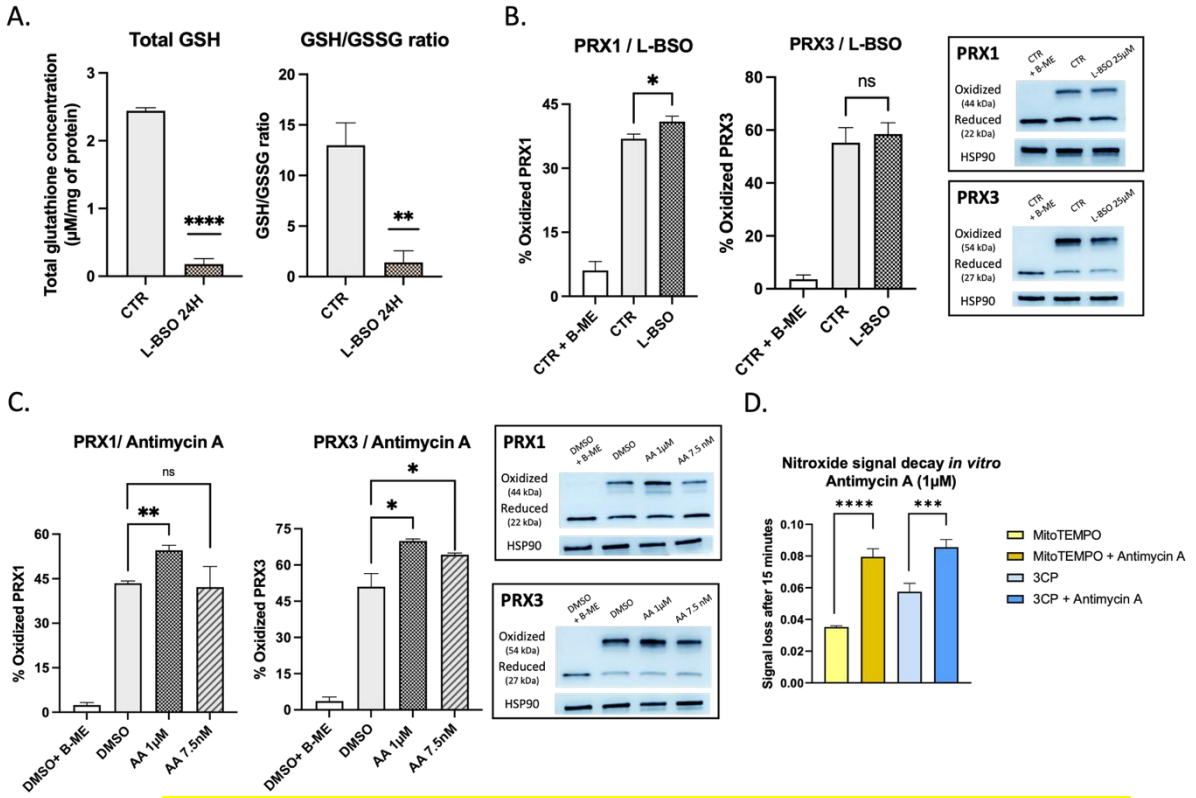

Figure S4.ROS production in different cellular compartments by L-BSO and Antimycin A in 4T1 cells.

(A) Total glutathione concentration and GSH/GSSG ratios in cells after L-BSO (25µM) treatment for 24 hours. Bars represent mean ± SEM. n=3 with 3 technical replicates, Student's T-test. **; $p < 0.01$, ****; $p < 0.001$

(B) Percentage of oxidation of PRX1 and PRX3 when cells are treated with L-BSO. CTR + B-ME = control group with ß-mercaptoethanol pre-treatment. CTR= control group. L-BSO = treated group with 25µM of L-BSO for 24 hours. Bars represent mean ± SEM. n=3 with 3 technical replicates, one-way ANOVA. ns= non significant, *; $p < 0.05$

(C) Percentage of oxidation of PRX1 and PRX3 when cells are treated with Antimycin A. DMSO + B-ME = control group (0.001% of DMSO) with ß-mercaptoethanol pre-treatment. DMSO = control group (0.001% of DMSO). AA 1µM= treated group with 1µM of Antimycin A for 24 hours. AA 7.5nM= treated group with 7.5nM Antimycin A for 24 hours. Bars represent mean ± SEM. n=3 with 3 technical replicates, one-way ANOVA. ns= non significant, *; $p < 0.05$, **; $p< 0.01$

(D) EPR signal loss after 15 minutes when 4T1 cancer cells were exposed to 1 µM of Antimycin A for 24 hours. Bars represent mean ± SEM. n = 3 with 3 technical replicates, one-way ANOVA, ***; $p < 0.005$, ****; $p < 0.001$

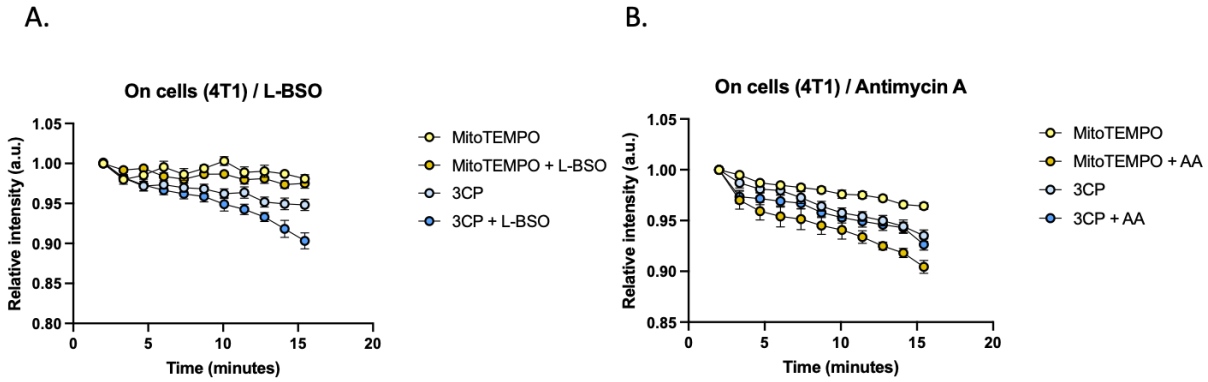

Figure S5. EPR signal decrease of 3CP and MitoTEMPO in 4T1 cells treated with L-BSO or Antimicyn A.

(A) Signal decay over time of MitoTEMPO and 3CP (20μM) when cells are treated with L-BSO (25μM) for 24 hours. n=3 with 3 technical replicates.

(B) Signal decay over time of MitoTEMPO and 3CP (20μM) when cells are treated with Antimycin A (AA, 7.5nM) for 24 hours. n=3 with 3 technical replicates.

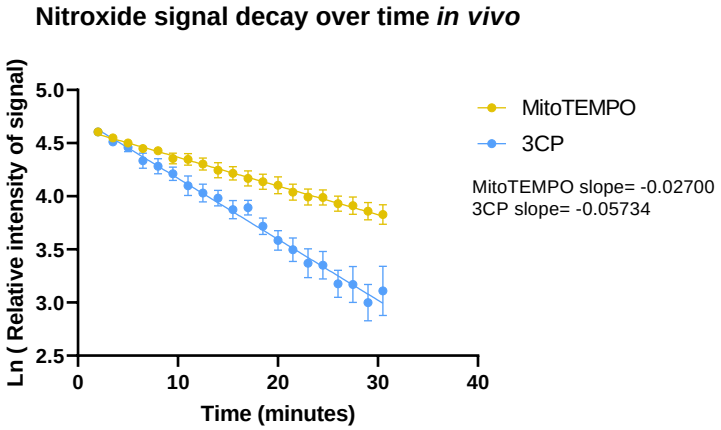

Figure S6. Kinetics of the decay of the EPR signal recorded in 4T1 tumors in mice (presented as the natural logarithm of the intensity over time). Points represent means ± SEM, n = 6/group.

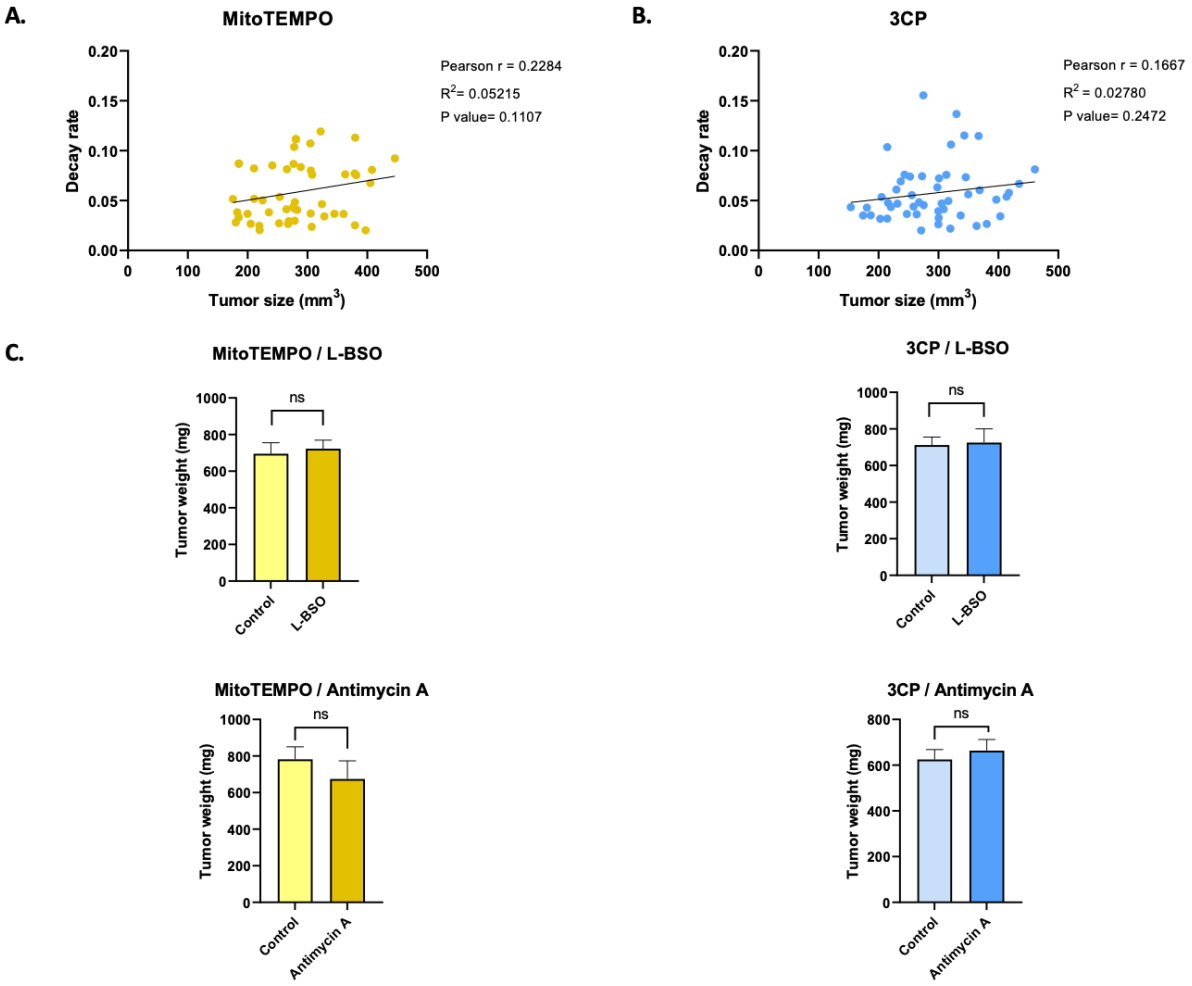

Figure S7. Absence of correlation between tumor size and EPR signal decay rate and tumor weights measured between the different groups.

(A) Absence of correlation between MitoTEMPO signal decay rate and tumor size. n=50, Pearson's correlation test

(B) Absence of correlation between 3CP signal decay rate and tumor size. n=50, Pearson's correlation test

(C) Tumor weights after mice were treated 72 hours with L-BSO (500mg/kg) or Antimycin A (0,3mg/kg). n=6/group. Student's t-test, ns; p >0.05

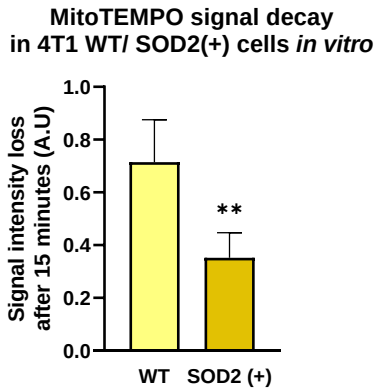

Figure S8. *In vitro* nitroxide signal loss of mitoTEMPO after 15 minutes for wild-type 4T1 cells and 4T1 cells overexpressing SOD2. Bars represent means ± SEM. N = 3, Student's t-test, **; $p < 0.01$.